
Rain Detection in the West African Sahel using Deep Learning on Satellite Imagery

by

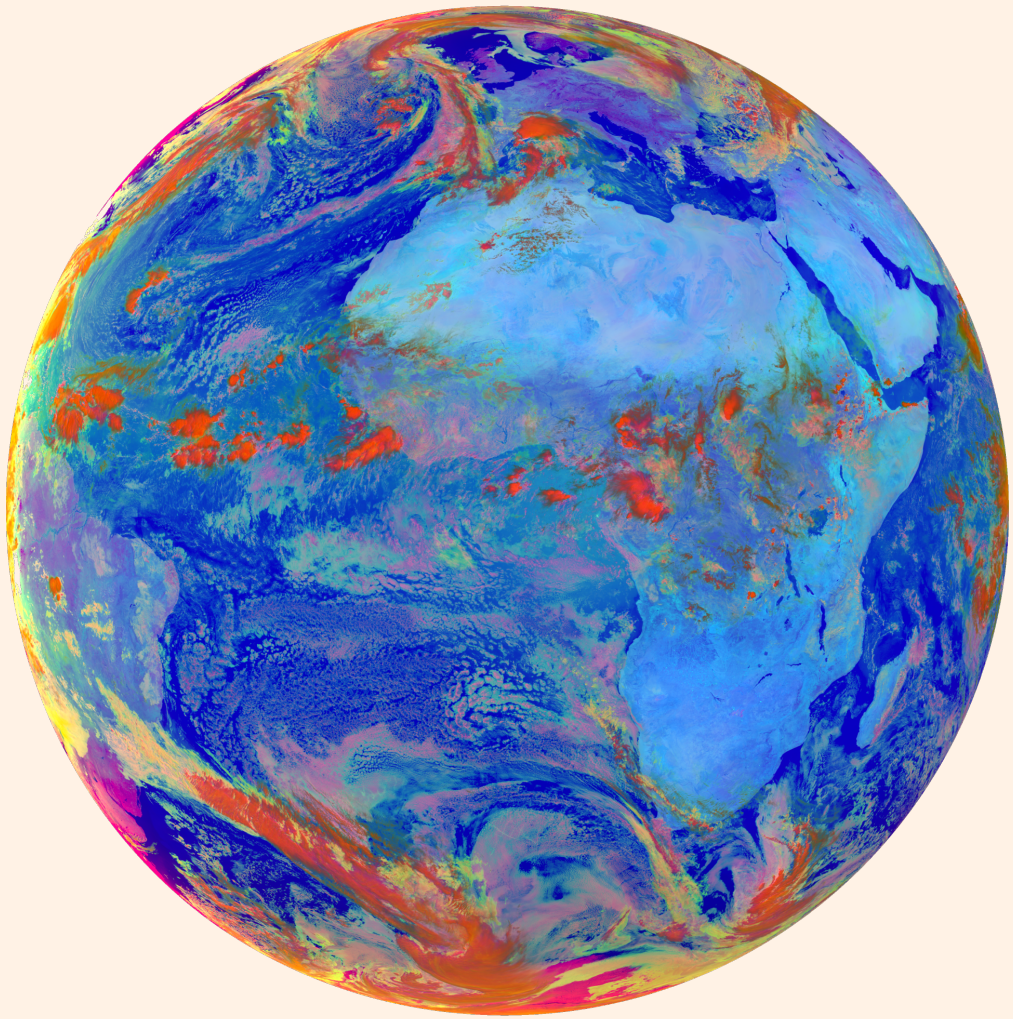
T.J. SIEBRING

to obtain the degree of Master of Science at
the VU Amsterdam and University of Amsterdam.

COMPUTER SCIENCE

Supervisor: Dr. A. Bon
Second reader: Prof. dr. J.M. Akkermans
Student number: 2683240
Year: 2024





Preface

I would like to express my gratitude first and foremost to Anna Bon. Your positive attitude and support for students and staff, under any circumstances, are inspirational. Secondly, I would like to thank Hans Akkermans, André Baart, Francis Dittoh, Gideon Ali and Spyros Paparrizos, for interesting discussions, and in particular André for his technical expertise. Lastly, I would like to thank my family and friends for their support - always.

*Go fast, go alone.
Go far, go together.*

The image on page i was captured by the SEVIRI instrument at 10:57 on September 21, 2019. The colours correspond to the Day Microphysics RGB Composite.

Rain Detection in the West African Sahel using Deep Learning on Satellite Imagery

T.J. Siebring

VU Amsterdam and University of Amsterdam

ABSTRACT

This study assesses the ability of a Deep Learning model to detect daytime rainfall in the West African Sahel using satellite imagery and ground observations. Specifically, we explore the effects of including various data sources as model inputs. The results show that best performance is achieved when information from both the infrared and near-visible spectrum are utilized.

KEYWORDS

Rain gauge; rain detection; deep learning; MSG SEVIRI; TAHMO; West Africa; convolutional neural network.

1 INTRODUCTION

A significant portion of the population in West Africa relies on subsistence farming, with agriculture predominantly rain-fed. This reliance is especially pronounced in the Sahel region, which has a single annual rain season. The timing of crop planting is therefore crucial, as the soil has been desiccated by the preceding dry season. For the seeds to take root, sufficient rainfall is necessary, in particular during the first days after seeding.

Weather agencies in the region typically use large-scale global models employing Numerical Weather Prediction (NWP) for forecasting. However, these models are primarily calibrated using data from more moderate climates, leading to inherent biases when applied to the extreme weather patterns of the Sahel, such as its north-south gradient. Sun et al. [23] provides a comprehensive evaluation of global rainfall products, identifying significant discrepancies in regions with sparse meteorological measurements. A region mentioned specifically is North Africa, which is known for its warm clouds - a cloud type that complicates rainfall estimation [13]. Calibration of these models using local data is therefore essential. However, this process is hindered by the limited availability of meteorological equipment as it is a low-resource environment.

Satellite-based precipitation products are widely used across the African continent. While these products demonstrate reasonable accuracy at dekadal (10-day) and monthly timescales, their performance on a daily basis is inadequate, as noted by [3 14 20]. This limitation significantly reduces their utility for local farmers, who require precise daily forecasts to make informed agricultural decisions.

To battle the data scarcity problem, the Trans-African Hydro-Meteorological Observatory (TAHMO) [25] was set up. A prototype of an acoustic disdrometer was developed in the Netherlands, which can be produced for less than one percent of the cost of a commercial equivalent with the same specifications [24]. Since inception, more than 500 stations have been installed throughout Africa, and five minute precipitation is automatically gathered in combination with many other variables. This is a significant improvement in terms of local data availability and quality in comparison to daily collected rainfall.

Estébanez-Camarena et al. [5] published a promising paper making use of this data for three hourly rainfall detection. The authors train a self designed Deep Learning (DL) model on eight TAHMO rain gauges in Northern Ghana. The model input is infrared radiation (IR) images from the Spinning Enhanced Visible and IR Imager (SEVIRI) instrument - a device onboard the Meteosat Second Generation (MSG) satellite that is commonly used for meteorological purposes. In a follow up work, the authors perform a similar analysis including another type of IR radiation. With these two input channels, they were able to achieve a rainfall Probability of Detection (POD) of 67 percent and False Alarm Ratio (FAR) of 59 percent [4]. This clearly demonstrates the potential of using satellite imagery for rainfall detection in West Africa.

In this study, we follow up on this work by:

- using ten input channels: two IR channels used by Estébanez-Camarena et al. [5], and eight other

channels commonly used in literature - seven IR and one visible and near infrared (VNIR);

- reducing the time step from three hours to one hour;
- studying the West African Sahel, including the North Ghanaian gauges;
- increasing the study period from 2018-2020 to 2018-2022;
- applying a widely used DL architecture for image classification.

The goal of these potential improvements is to answer the research questions:

- (1) Can the benchmark for rainfall detection in the West African Sahel be improved by incorporating additional data sources?
- (2) Will this be enough to help farmers in the West African Sahel with their decision making process?

2 DATA

2.1 TAHMO Rain Gauges

TAHMO provided hourly rain data for 61 stations in West Africa for the period July 2018 to December 2022. The locations corresponding to the TAHMO weather stations are displayed in Figure 1. As the study area covers multiple time zones, timestamps were adjusted accordingly.

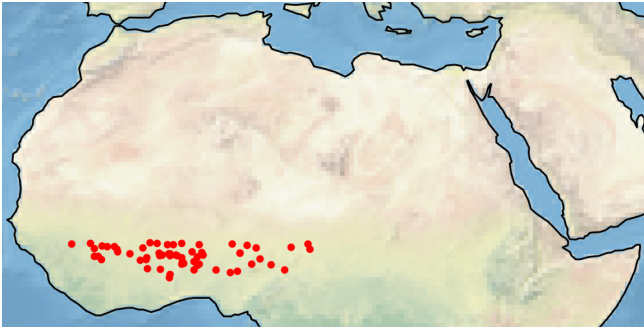


Figure 1: Locations corresponding to TAHMO weather stations in data set.

Due to significant variation in data availability across stations, we established a minimum threshold of 20 percent, resulting in a total of 51 stations being included in the analysis. All subsequent metrics are based on this selection. 20 percent is a relatively low threshold, and 51 stations represent a modest number of gauges

for such a large region, which becomes particularly evident when compared to studies conducted in the Global North. For instance, Moraux et al. [16] utilized 1,176 high-availability gauges for their research in Germany, Belgium, and the Netherlands - a region much smaller than our study area. This comparison underscores the importance of both a high number of gauges and high quality data for each gauge, which is common in the Global North but rare on the African continent. Figure 3 illustrates data availability, sorted from high to low. Increasing the threshold to 50 or 80 percent would significantly reduce the number of gauges available for analysis. All missing data have been excluded from the dataset.

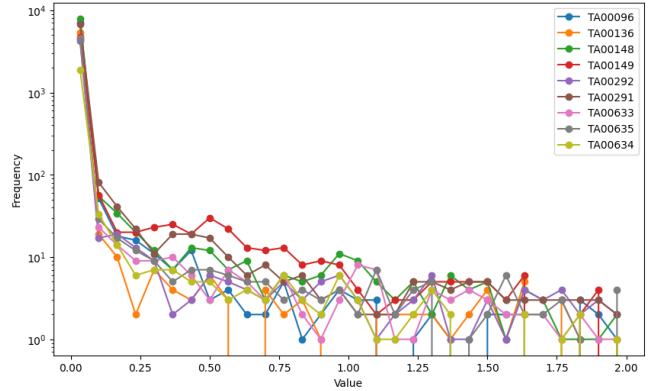


Figure 2: Logarithmic frequency distribution of measured rainfall in mm/h.

For each weather station, precipitation in mm per hour is available, amongst other variables such as longitude, latitude and elevation. As the goal is to detect rain, we need to decide upon a threshold for rain/no-rain. Figure 2 shows the logarithmic frequency distribution for a selection of nine gauges. No clear cutoff point can be observed, so we decide to use a threshold of 0.4mm/h for data preparation. However, we maintain the original rainfall rate for future analysis for each data point. Using this threshold, we obtain a ratio rain:no-rain of 1:49. In Section 3.1 we discuss how we preprocess this severely skewed data set.

To include temporal information, the transformations (1) and (2) are applied to the daily and yearly time stamp, ensuring continuity. We prefer the cosine over sine as the daily and yearly extremes are reached around 00:00, 12:00, and January, July, respectively. The 0.5 is included to ensure we take the middle of the hour and

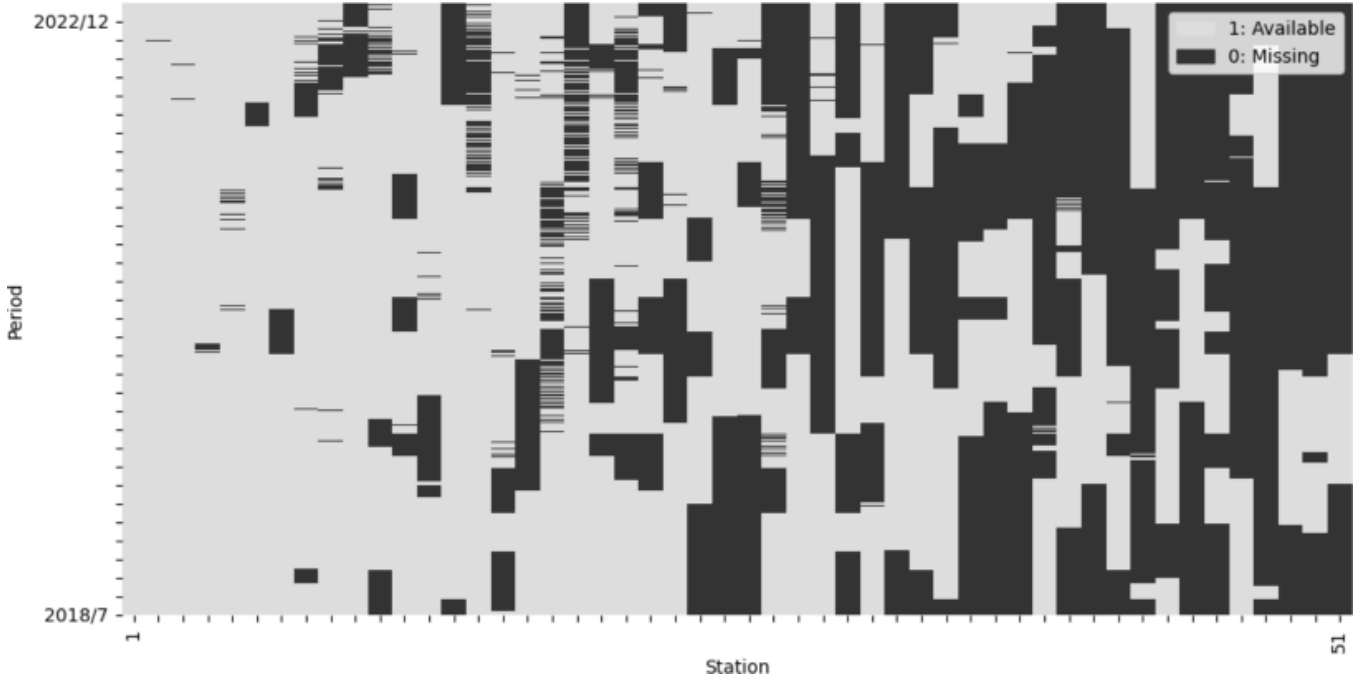


Figure 3: Data availability for TAHMO stations with at least 20% data, sorted from high to low availability.

day, respectively. The 2π is evidently added to convert the ratio to radians. Lastly, $days_in_year$ was used to account for the extra day in 2020.

$$time_of_day = \cos \left[2\pi \cdot \frac{hour_of_day + 0.5}{24} \right] \quad (1)$$

$$time_of_year = \cos \left[2\pi \cdot \frac{day_of_year - 0.5}{days_in_year} \right] \quad (2)$$

2.2 SEVIRI Satellite Images

Level 1.5 images are used from the SEVIRI instrument. It has twelve spectral channels, eight of which are in the IR region of the electromagnetic spectrum. These can provide information on temperature of objects such as clouds, amongst other things. The imaging component of the instrument spins at 100 rpm, scanning the earth one slice at a time. Every twelve minutes the device goes from south to north, after which it takes three minutes to adjust south again. Therefore, the temporal resolution is fifteen minutes. The spatial resolution is 3x3km per pixel at nadir. As the nadir is located at latitude 0 and longitude 0, and the proximity of our study

area to this point, for practical purposes our spatial resolution is also 3x3km. All processing of SEVIRI images is performed using the Python library *Satpy*.

The purpose of using satellite images is to get information about low level clouds, as these can produce rain. Therefore, images that are sensitive to radiation with a large atmospheric transmissivity are desired, as these have the highest probability of containing information about clouds producing rainfall. For the SEVIRI instrument, the 10.8 micron channel is therefore commonly used [10].

Estébanez-Camarena et al. [5] solely uses this channel in their original work, only to add the 7.3 micron channel in their follow up study, as it interacts with water vapour (WV) [4]. There is one other SEVIRI WV channel of 6.2 micron - located in the middle of the WV absorption band. The authors therefore argue that the 7.3 channel is more suited for rainfall estimation, as it has a larger WV transmissivity. In contrast, Moraux et al. [16] decided to use the 8.7 and 12.0 besides the 10.8 channel, as these three channels are well-known to be related to cloud top particle size, temperature and cloud optical thickness [12]. To better understand the influence of these channels, all four channels are included in

this research. In particular, their corresponding Brightness Temperatures (BT) [21] are extracted.

Additionally, the RGB composite Desert Dust is included, which could be relevant in our study area right below the Sahara desert [1]. Its primary aim is detecting dust in the atmosphere, and it is a function of the 8.7, 10.8 and 12.0 channels, with three (RGB) outputs [8]. Lastly, the RGB composite Day Microphysics is included, as its primary aim is to distinguish ice from water, and to provide information on cloud top particle size, temperature and cloud optical thickness [7]. Interestingly, this composite uses the visible 0.8 and infrared 3.9 channels, in contrast to the commonly used 8.7, 10.8 and 12.0 channels for the 24-hour Microphysics RGB composite [6]. As the composite depends on a channel close to the visible spectrum, it can only be used during daytime, halving our data set in effect. However, it uses new channels that are not included in our selection so far, and it is more commonly used for daytime specific rainfall analysis [2].

In total, this yields ten input channels: four BTs and two RGB composites. An overview of their corresponding underlying SEVIRI spectral channels is provided in Table 1, including corresponding spectral bandwidths.

ID	Centre (μm)	Min (μm)	Max (μm)
VIS 0.8	0.810	0.74	0.88
IR 3.9	3.920	3.48	4.36
IR 7.3	7.350	6.85	7.85
IR 8.7	8.700	8.30	9.10
IR 10.8	10.800	9.80	11.80
IR 12.0	12.000	11.00	13.00

Table 1: SEVIRI spectral channels used in this research, with corresponding nominal centre wavelengths and spectral bandwidths [9].

As our study period is July 2018 to December 2022, most images originate from the MSG 4 satellite. However, a small part originates from MSG 2 and MSG 3. No significant differences between these images were found. Partly missing or duplicate data were not included. In total approximately 45 TB was downloaded using the EUMETSAT API¹ in November 2023. Given the large quantity of data, high bandwidth Virtual Machines (VMs) on Google Cloud Platform (GCP)’s Compute Engine were used to achieve this task. Data was

¹<https://api.eumetsat.int>

shortly stored on Persistent Disks to reduce retrieval times for processing, as discussed in Section 2.3.

2.3 Matching Images with Gauges

To estimate hourly rain/no-rain measured by a gauge using SEVIRI images, we need to collect the relevant pixels for each gauge and timestamp. Consequently, for each gauge location we take the closest 32x32 grid of SEVIRI pixels as shown in Figure 4, for each of the ten input channels discussed in Section 2.2, and for each four images per hour. Note that because of this decision, the grid points are not equidistant to the TAHMO station, as shown by the red dot slightly deviating from the central intersection. However, in favour of speed, and testing robustness later on, we decided not to interpolate.

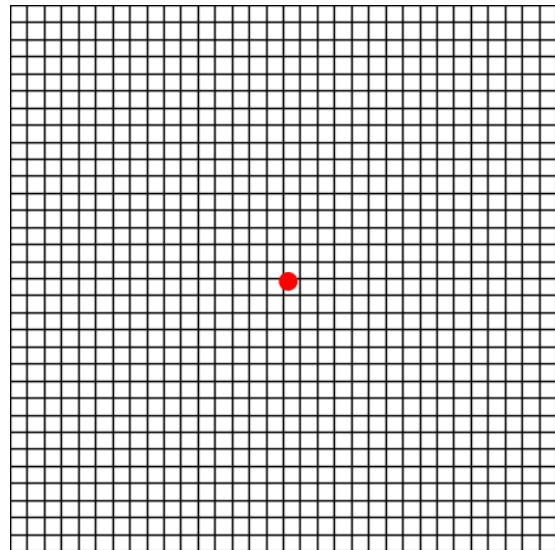


Figure 4: TAHMO gauge surrounded by the closest 32x32 grid of SEVIRI pixels.

As for the download task, we use multiple VM instances on GCP’s Compute Engine to process the 45TB of images to approximately 500GB of 4 dimensional tensors of shape $10 \times 4 \times 32 \times 32$. To speed up this process we use SSDs as Persistent Disk, and after profiling we were able to reduce the processing time to seconds per image. With 160k images and multiple VMs this yields a feasible processing time. We store the resulting tensors in a Bucket on GCP’s Cloud Storage.

3 METHODOLOGY

3.1 Data Preprocessing

For the train, validation and test set we use 80/10/10 percent of data, respectively. To split up the data, several considerations need to be taken into account. To prevent fitting to specific weather stations, ideally we perform validation and testing on weather stations on which no training occurred. However, as the data entails 51 stations, this would imply 10 stations for validation and testing. This is undesired as the density of stations over the study area is already low, and large differences exist in data availability between the stations. Meanwhile, we need to take into account that there is a high correlation between two subsequent data points. Using one in training and the other in testing is unacceptable. Furthermore, all three data sets should be representative for each time of the day and year. Therefore, as the study period is almost 5 years and we are interested in 4/5th of the data for training, we designed Algorithm 1 to solve these constraints.

Algorithm 1 Data Splitting for Training, Validation, and Testing.

```
for each unique date  $d$  in the study period do  
  if  $(year(d) + day\_in\_year(d)) \bmod 5 \neq 0$  then  
    Assign  $d$  to Train set  
  else if  $(year(d) + day\_in\_year(d)) \bmod 10 = 0$   
  then  
    Assign  $d$  to Validation set  
  else  
    Assign  $d$  to Test set  
  end if  
end for
```

The data imbalance of 1:49 as discussed in Section 2.1 poses significant challenges for training machine learning models effectively. A commonly employed strategy to mitigate this issue is to oversample the positive class (rain) or undersample the negative class (no-rain) in the training data. We decide to go for the latter, randomly reducing the no-rain occurrences to 1/5th of the original size, improving the ratio to 1:10. The validation and test set remain unaffected.

Lastly, to standardise the SEVIRI images we calculate the ten channel-specific means and standard deviations from the training set. These are subsequently used to

also standardize the validation and test set on a per channel basis. The values are clamped at $[-4, 4]$.

3.2 Model Inputs

The data sources outlined in Table 2 serve as model inputs for hourly rain detection, with corresponding domains before preprocessing. Note that due to the inclusion of the Day Microphysics RGB Composite, we exclude all data outside the daily time interval of 7:00-19:00.

Model input	Domain
BT of 7.3, 8.7, 10.8 and 12.0 channels	$\mathbb{R}_+^{4 \times 4 \times 32 \times 32}$
Desert Dust RGB Composite	$\mathbb{R}^{3 \times 4 \times 32 \times 32}$
Day Microphysics RGB Composite	$\mathbb{R}^{3 \times 4 \times 32 \times 32}$
Elevation	\mathbb{R}
Time of day	$(-1, 1)$
Time of year	$(-1, 1)$

Table 2: Model inputs with corresponding domains used for hourly rainfall detection.

3.3 Model Architecture

In regions with abundant meteorological data, the use of Machine Learning techniques for rainfall estimation has been well-established for over a decade. Notably, the rapid advancements in image classification due to the introduction of Convolutional Neural Networks (CNN), have significantly bolstered the use of satellite-based rainfall estimation techniques. Already in 2016, Meyer et al. [15] showed that fairly rudimentary DL techniques outperform conventional Machine Learning techniques such as Random Forests in estimating rainfall over Germany using SEVIRI imagery. Fast forward three years, and Moraux et al. [16] employs an advanced encoder-decoder architecture, similar to the U-Net architecture that originated in biomedical image segmentation [19], mapping SEVIRI images to pixelated gauge images. Combined with gauge interpolation and orographic information, the paper shows good nowcasting results.

In a follow up work, Moraux et al. [17] show that by also including radar, performance is enhanced significantly. Similarly, van der Kooij [26] uses radar to nowcast heavy precipitation events in the Netherlands.

Input channels	AUPRC	POD	1-FAR	F1 Score	ACC
BT 7.3, 10.8	0.31	0.46	0.24	0.29	0.97
BT 8.7, 10.8, 12.0	0.34	0.43	0.25	0.29	0.97
Desert Dust RGB Composite	0.32	0.44	0.26	0.31	0.97
Day Microphysics RGB Composite	0.39	0.50	0.25	0.32	0.97
All ten channels	0.37	0.47	0.27	0.32	0.97

Table 3: Performance metrics for different input channels.

The author uses the Trajectory Gated Recurrent Unit (TrajGRU) DL architecture that was developed by Shi et al. [22] to actively learn location variant structures for recurrent connections, i.e. capture trajectory patterns. Xu et al. [27] also uses TrajGRU as a first stage, showing good performance in capturing rain field trajectories. The authors subsequently combine an attention module with a Generative Adversarial Network model using a U-Net structure for the second stage, outperforming comparable studies.

Although these architectures achieve strong results, they are built on large data sets, usually involving radar. More data allows for more complex model architectures, but in our case we have orders of magnitude less data. Employing these elaborate architectures could therefore lead to rapid overfitting. Therefore, we resort to an older, widely used CNN architectures for classification tasks that requires less data for training than the previously described architectures: ResNet [11].

Specifically, we use two groups of three Pre-Activation ResNet blocks of resolution 32×32 for the first group and 16×16 for the second. In the last layer, adaptive average pooling is applied and the time stamps and elevation are added in a subsequent fully connected layer of size 64. The total number of parameters in this setup is approximately 67k, depending on the number of input channels. Due to the low density of rain gauges in our study area, we opted not to include gauge interpolation as a model input.

4 RESULTS

To evaluate the model, we utilized the test dataset. All training was conducted exclusively using the training and validation datasets. Given the highly imbalanced data, performance was assessed using the Area Under the Precision-Recall Curve (AUPRC) metric. Additionally, we report the Probability of Detection (POD), False

Alarm Rate (FAR), Accuracy (ACC), and F1 Score, derived from the model’s contingency table. Logging was performed using *Weights and Biases*².

The results are obtained using a one GTX 1070 8GB GPU with 32GB of RAM. We use the python library *PyTorch*, and in particular *PyTorch Lightning*, to instruct the GPU.

For the ResNet architecture, we experimented with different group sizes and resolutions, with the current setup yielding the highest performance. Both the AdamW and SGD optimizer were tested, with AdamW giving the best performance overall. Therefore, all reported results use the AdamW optimizer.

To further correct for the data imbalance, we use a class weight of 1.5 for rain events. The batch size is 512, and we run 50 epochs for each experiment. We clip the gradient at 1, and for the learning rate we employ a 5 step decay strategy. For the loss function we use Binary Cross Entropy on the logits. For each experiment, the best performing model in terms of minimal validation loss are saved.

No data augmentation was done, as our region of interest is bordered by the Sahara at the top and the Atlantic Ocean at the bottom, yielding significantly different meteorological dynamics. Experiments were carried out moving the rain/no-rain threshold to values higher and lower than 0.4, as discussed in Section 2.1. However, no significant differences in performance were found.

To demonstrate the effect on performance when using different input channels, first the input channels of Estébanez-Camarena et al. [4] and Moraux et al. [16] are evaluated. Subsequently, the Desert Dust and Day Microphysics RGB composites are tested, and lastly all ten channels combined. The results are presented in Table 3.

²<https://wandb.ai>

5 DISCUSSION

This study follows up on the promising work of Estébanez-Camarena et al. [5] and corresponding follow up study [4]. Although we use more gauges, cover a larger time period, include elevation, and use a widely used deep learning architecture for classification, the results show worse performance which we cannot fully explain. We do note that as we employ a time step of one hour instead of three hours, performance is adversely affected. Nonetheless, a POD of 0.50 and FAR of 0.75 is insufficient for practical purposes. Initially we tried rebuilding the architecture from Estébanez-Camarena et al. [4] with 11 million parameters. However, we were not able to reproduce the results. Due to strong signs of overfitting we adapted a smaller, different architecture with approximately 67 thousand parameters.

Besides the time step argument, performance might also be negatively affected due to the inclusion of gauges spanning a much larger area than the relatively dense gauges in Northern Ghana. Furthermore, despite Figure 3 not indicating this directly, most of the low availability gauges are located outside of Ghana - with the Ghanaian gauges employed by Estébanez-Camarena et al. [4] having relatively high availability. The inclusion of these low quality gauges might have added extra noise to the measurements. Lastly, while ResNet is a well-known and broadly cited architecture for classification tasks, it remains a general architecture that was not specifically designed for capturing spatiotemporal patterns. Perhaps architectures specifically designed for this task, such as the encoder stage of the TrajGRU architecture [22], yield better performance.

An intriguing result of our study is that the model exhibits its lowest performance on the channels utilised by Estébanez-Camarena et al. [4]. This suggests that incorporating additional channels could enhance their model's performance. Although the differences in performance between our models are minor, the results indicate that during daytime, most cloud information is captured by including information from the near-visible spectrum. This underscores the potential advantage of developing separate rainfall estimation models for daytime and nighttime. A contributing factor to this observation could also be that information from the near-visible spectrum was included using a composite product. As discussed in Section 2.2, composites incorporate meteorological information that the

model therefore need not learn independently. Perhaps including these patterns directly in the source data is beneficial in studies where limited data is available. A result challenging this observation is the slightly worse performance of the Desert Dust composite with respect to its underlying raw channels, specifically the 8.7, 10.8 and 12.0 micron channels. Namely, despite being designed to recognize dust, it is very similar to the 24h Microphysics composite [6 8]. Lastly, including all ten channels did not improve overall performance, which shows that adding additional input data need not yield better results.

However, perhaps most important is the data constraint faced in the West African Sahel. Moraux et al. [16] uses very high quality 5-minute data of more than a thousand gauges in a region significantly smaller than our study area. They achieve a POD and FAR of 0.47 and 0.63, respectively, using the BTs of the 8.7, 10.8 and 12.0 channels. Additionally, due to the high gauge density, they also performed gauge interpolation, increasing the performance to a POD of 0.75/0.84 and FAR of 0.30/0.10 on a 5-minute/daily time step, respectively. This demonstrates the potential of having a high density gauge network, and therefore also the urgency for the West African Sahel and the African continent generally to boost the number of weather stations available.

Now we do note that are already many stations available. TAHMO is one such example, but there are numerous others, such as national weather agencies. Combining these data sources could bring data conditions and therefore model performance closer to those observed in the West. Perhaps even different types of data such as soil moisture [18] could be of use. Therefore we highly urge the data controlling agencies in this field to make the data easily accessible for research purposes, as this would allow for multi-source studies instead of commonly observed single-source studies such as this one. However, at this point we recommend future work to focus solely on small densely gauged regions, employing a daily time step or larger. Lastly, new data sources such as Meteosat Third Generation, which have better spatial and temporal resolution, or inclusion of radar [17] could boost performance.

6 CONCLUSION

This study examines whether the benchmark for rainfall detection in the West African Sahel can be improved by

incorporating a wider array of data inputs. By leveraging more channels of the SEVIRI instrument, including both infrared and near-visible, we aim to enhance the accuracy of a Deep Learning model in detecting daytime rainfall, evaluated on ground observations. The results show that best performance is achieved when information from both the infrared and near-visible spectrum are utilized. Interestingly, despite the proximity of our study area to the Sahara Desert, including information indicative of desert dust did not enhance performance. Nevertheless, model accuracy is insufficient for practical purposes.

The primary challenge in this region remains the limited availability of high-quality meteorological data. The difficulties associated with improving data quality and increasing the number of weather stations underscore the need for more accessible local data that is already available. Improving data accessibility would not only support the development of more accurate weather models, but also enhance the capacity for researchers to address the unique climatic challenges faced by the West African Sahel.

7 ACKNOWLEDGEMENTS

We want to firstly thank M. Estébanez-Camarena of Delft University of Technology for the support of this work and fruitful discussions; secondly TAHMO for providing the gauge data; thirdly Université Paris Est Créteil for providing compute resources; lastly the research environment provided by EURIDICE³.

REFERENCES

- [1] Jamie R. Banks, Anja Hünerbein, Bernd Heinold, Helen E. Brindley, Hartwig Deneke, and Kerstin Schepanski. 2019. The sensitivity of the colour of dust in MSG-SEVIRI Desert Dust infrared composite imagery to surface and atmospheric conditions. *Atmospheric Chemistry and Physics* 19, 10 (May 2019), 6893–6911. <https://doi.org/10.5194/acp-19-6893-2019> Publisher: Copernicus GmbH.
- [2] R. S. Chadwick, D. I. F. Grimes, R. W. Saunders, P. N. Francis, and T. A. Blackmore. 2010. The TAMORA algorithm: satellite rainfall estimates over West Africa using multi-spectral SEVIRI data. *Advances in Geosciences* 25 (March 2010), 3–9. <https://doi.org/10.5194/adgeo-25-3-2010> Conference Name: Precipitation: Measurement, Climatology, Remote Sensing, and Modeling (EGU Session 2009) - EGU General Assembly 2009, Vienna, Austria, 19–24 April 2009 Publisher: Copernicus GmbH.
- [3] Moctar Dembélé and Sander J. Zwart. 2016. Evaluation and comparison of satellite-based rainfall products in Burkina Faso, West Africa. *International Journal of Remote Sensing* 37, 17 (Sept. 2016), 3995–4014. <https://doi.org/10.1080/01431161.2016.1207258>
- [4] Mónica Estébanez-Camarena, Fabio Curzi, Riccardo Taormina, Nick van de Giesen, and Marie-Claire ten Veldhuis. 2023. The Role of Water Vapor Observations in Satellite Rainfall Detection Highlighted by a Deep Learning Approach. *Atmosphere* 14, 6 (June 2023), 974. <https://doi.org/10.3390/atmos14060974> Number: 6 Publisher: Multidisciplinary Digital Publishing Institute.
- [5] Mónica Estébanez-Camarena, Riccardo Taormina, Nick van de Giesen, and Marie-Claire ten Veldhuis. 2023. The Potential of Deep Learning for Satellite Rainfall Detection over Data-Scarce Regions, the West African Savanna. *Remote Sensing* 15, 7 (Jan. 2023), 1922. <https://doi.org/10.3390/rs15071922> Number: 7 Publisher: Multidisciplinary Digital Publishing Institute.
- [6] EUMETRAIN. 2017. SEVIRI 24-hour Microphysics RGB Quick Guide. https://resources.eumetrain.org/rgb_quick_guides/quick_guides/24MicroRGB.pdf.
- [7] EUMETRAIN. 2017. SEVIRI Day Microphysics RGB Quick Guide. https://resources.eumetrain.org/rgb_quick_guides/quick_guides/DaymicroRGB.pdf.
- [8] EUMETRAIN. 2017. SEVIRI Dust RGB Quick Guide. https://resources.eumetrain.org/rgb_quick_guides/quick_guides/DustRGB.pdf.
- [9] EUMETSAT. 2017. MSG Level 1.5 Image Data Format Description. https://www-cdn.eumetsat.int/files/2020-05/pdf_ten_05105_msg_img_data.pdf.
- [10] U. Hamann, A. Walther, B. Baum, R. Bennartz, L. Bugliaro, M. Derrien, P. N. Francis, A. Heidinger, S. Joro, A. Kniffka, H. Le Gléau, M. Lockhoff, H.-J. Lutz, J. F. Meirink, P. Minnis, R. Palikonda, R. Roebeling, A. Thoss, S. Platnick, P. Watts, and G. Wind. 2014. Remote sensing of cloud top pressure/height from SEVIRI: analysis of ten current retrieval algorithms. *Atmospheric Measurement Techniques* 7, 9 (Sept. 2014), 2839–2867. <https://doi.org/10.5194/amt-7-2839-2014>
- [11] Kaiming He, Xiangyu Zhang, Shaoqing Ren, and Jian Sun. 2015. Deep Residual Learning for Image Recognition. <http://arxiv.org/abs/1512.03385> arXiv:1512.03385 [cs].
- [12] I. M. Lensky and D. Rosenfeld. 2008. Clouds-Aerosols-Precipitation Satellite Analysis Tool (CAPSAT). *Atmospheric Chemistry and Physics* 8, 22 (Nov. 2008), 6739–6753. <https://doi.org/10.5194/acp-8-6739-2008> Publisher: Copernicus GmbH.
- [13] Viviana Maggioni, Patrick C. Meyers, and Monique D. Robinson. 2016. A Review of Merged High-Resolution Satellite Precipitation Product Accuracy during the Tropical Rainfall Measuring Mission (TRMM) Era. *Journal of Hydrometeorology* 17, 4 (April 2016), 1101–1117. <https://doi.org/10.1175/JHM-D-15-0190.1>
- [14] Kirubel Mekonnen, Naga Manohar Velpuri, Mansoor Leh, Komlavi Akpoti, Afua Owusu, Primrose Tinonetsana, Tarek Hamouda, Benjamin Ghansah, Thilina Prabhath Paranamana,

³<https://euridice.eu>

- and Yolande Munzimi. 2023. Accuracy of satellite and re-analysis rainfall estimates over Africa: A multi-scale assessment of eight products for continental applications. *Journal of Hydrology: Regional Studies* 49 (Oct. 2023), 101514. <https://doi.org/10.1016/j.ejrh.2023.101514>
- [15] Hanna Meyer, Meike Kühnlein, Tim Appelhans, and Thomas Nauss. 2016. Comparison of four machine learning algorithms for their applicability in satellite-based optical rainfall retrievals. *Atmospheric Research* 169 (2016), 424–433. <https://doi.org/10.1016/j.atmosres.2015.09.021>
- [16] Arthur Moraux, Steven Dewitte, Bruno Cornelis, and Adrian Munteanu. 2019. Deep Learning for Precipitation Estimation from Satellite and Rain Gauges Measurements. *Remote Sensing* 11, 21 (Jan. 2019), 2463. <https://doi.org/10.3390/rs11212463> Number: 21 Publisher: Multidisciplinary Digital Publishing Institute.
- [17] Arthur Moraux, Steven Dewitte, Bruno Cornelis, and Adrian Munteanu. 2021. A Deep Learning Multimodal Method for Precipitation Estimation. *Remote Sensing* 13 (Aug. 2021), 3278. <https://doi.org/10.3390/rs13163278>
- [18] Thierry Pellarin, Alexandre Zoppis, Carlos Román-Cascón, Yann H. Kerr, Nemesio Rodriguez-Fernandez, Jeremy Panthou, Nathalie Philippon, and Jean-Martial Cohard. 2022. From SMOS Soil Moisture to 3-hour Precipitation Estimates at 0.1° Resolution in Africa. *Remote Sensing* 14, 3 (Jan. 2022), 746. <https://doi.org/10.3390/rs14030746> Number: 3 Publisher: Multidisciplinary Digital Publishing Institute.
- [19] Olaf Ronneberger, Philipp Fischer, and Thomas Brox. 2015. U-Net: Convolutional Networks for Biomedical Image Segmentation. In *Medical Image Computing and Computer-Assisted Intervention – MICCAI 2015*, Nassir Navab, Joachim Hornegger, William M. Wells, and Alejandro F. Frangi (Eds.). Vol. 9351. Springer International Publishing, Cham, 234–241. https://doi.org/10.1007/978-3-319-24574-4_28 Series Title: Lecture Notes in Computer Science.
- [20] Frédéric Satgé, Dimitri Defrance, Benjamin Sultan, Marie-Paule Bonnet, Frédérique Seyler, Nathalie Rouché, Fabrice Pierron, and Jean-Emmanuel Paturel. 2020. Evaluation of 23 gridded precipitation datasets across West Africa. *Journal of Hydrology* 581 (Feb. 2020), 124412. <https://doi.org/10.1016/j.jhydrol.2019.124412>
- [21] Johannes Schmetz, Paolo Pili, Stephen Tjemkes, Dieter Just, Jochen Kerkmann, Sergio Rota, and Alain Ratier. 2002. SEVIRI CALIBRATION. (2002). https://www-cdn.eumetsat.int/files/2020-04/pdf_sci_bams0702_msg-calib.pdf
- [22] Xingjian Shi, Zhihan Gao, Leonard Lausen, Hao Wang, Dit-Yan Yeung, Wai-kin Wong, and Wang-chun Woo. 2017. Deep Learning for Precipitation Nowcasting: A Benchmark and A New Model. <http://arxiv.org/abs/1706.03458> arXiv:1706.03458 [cs].
- [23] Qiaohong Sun, Chiyuan Miao, Qingyun Duan, Hamed Ashouri, Soroosh Sorooshian, and Kuo-Lin Hsu. 2018. A Review of Global Precipitation Data Sets: Data Sources, Estimation, and Intercomparisons. *Reviews of Geophysics* 56, 1 (March 2018), 79–107. <https://doi.org/10.1002/2017RG000574>
- [24] TAHMO. August 2024. Website. <https://tahmo.org>
- [25] Nick Van De Giesen, Rolf Hut, and John Selker. 2014. The Trans-African Hydro-Meteorological Observatory. *WIREs Water* 1, 4 (July 2014), 341–348. <https://doi.org/10.1002/wat2.1034>
- [26] Eva van der Kooij. 2021. Nowcasting heavy precipitation in the Netherlands: a deep learning approach. (2021). <https://repository.tudelft.nl/islandora/object/uuid%3A536b1a77-625c-4476-9354-4d5b259a1080>
- [27] Liujia Xu, Dan Niu, Tianbao Zhang, Pengju Chen, Xunlai Chen, and Yinghao Li. 2022. Two-Stage UA-GAN for Precipitation Nowcasting. *Remote Sensing* 14, 23 (Jan. 2022), 5948. <https://doi.org/10.3390/rs14235948> Number: 23 Publisher: Multidisciplinary Digital Publishing Institute.